Available online at www.sciencedirect.com
SCIENCE DIRECT®
Computers and Structures 83 (2005) 383–393
Computers & Structures
www.elsevier.com/locate/compstruc

Ultimate limit state design of sheet pile walls by finite elements and nonlinear programming

Kristian Krabbenhoft [a], Lars Damkilde [b,*], Sven Krabbenhoft [b]

[a] Department of Civil Engineering, Technical University of Denmark, DK-2800 Lyngby, Denmark
[b] Institute of Chemistry and Applied Engineering Science, Section for Structural Mechanics, Aalborg University Esbjerg, Niels Bhor Vej 8, DK-6700 Esbjerg, Denmark

Received 16 December 2002; accepted 9 August 2004

Abstract

The design of sheet pile walls by lower bound limit analysis is considered. The design problem involves the determination of the necessary yield moment of the wall, the wall depth and the anchor force such that the structure is able to sustain the given loads. This problem is formulated as a nonlinear programming problem where the yield moment of the wall is minimized subject to equilibrium and yield conditions. The finite element discretization used enables exact fulfillment of these conditions and thus, according to the lower bound theorem, the solutions are safe.

Keywords: Sheet pile walls; Plasticity; Limit analysis; Material optimization; Finite elements; Nonlinear programming

1. Introduction

Limit analysis has been used for decades in civil and mechanical engineering practice as a means of analyzing structures of materials which with reasonable accuracy can be described as being rigid-perfectly plastic. Such materials include steel, concrete and soils. Traditionally, most attention has been given to the problem which consists of determining the ultimate magnitude of a given set of loads acting on a structure with a given geometry. This problem is relevant when determining e.g. the necessary extrusion pressure in metal forming problems, when evaluating the bearing capacity of reinforced concrete slabs or the stability of slopes, and generally, whenever all information about the structure, except for the ultimate magnitude of the load set, is known. However, in the design of structures the situation is the opposite. Here the loads are known whereas the necessary dimensions, boundary conditions, material strengths, etc. must be determined in such a way that the structure is able to sustain the given loads. Thus, limit analysis embraces two different scenarios, one where everything except the maximal permissible load intensity is known, and one where all that is known is the load intensity.

In the following we consider the latter of these problems with particular reference to the design of sheet pile walls. The example problem which we will return to in Section 7 is sketched in Fig. 1. Given the weight of the soil and the relevant strength parameters, for the Mohr–Coulomb criterion the cohesion and the angle of friction, the task is to determine the necessary yield

* Corresponding author. Tel.: +45 7912 7648; fax: +45 7545 3643.
E-mail address: ld@aaue.dk (L. Damkilde).

0045-7949/$ - see front matter © 2004 Elsevier Ltd. All rights reserved.
doi:10.1016/j.compstruc.2004.08.016

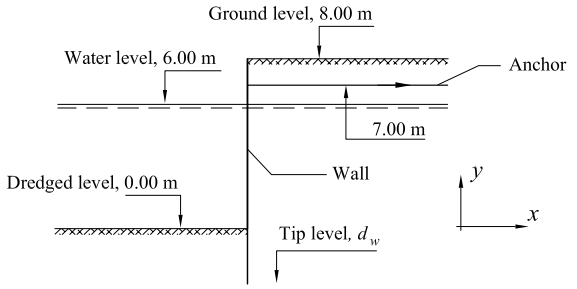

Fig. 1. Sheet pile wall.

moment of the wall, the anchor force, and the depth of the wall.

2. Problem formulation

The theorems of limit analysis provide powerful tools for the design and analysis of a wide variety of structures. Originally, hand calculations were used, and numerous methods have been developed. Although based on a common foundation, namely the limit theorems, these methods usually take quite different forms depending on the particular problem in question.

With the development of the modern computer it has become possible to generalize the hand calculation methods in terms of methods suited for large numerical computations. As with most hand calculation methods the numerical computations are based on either the upper or the lower bound theorem, and are carried out as optimizations.

Whereas the problem of determining the ultimate magnitude of a given load set has received considerable attention less work has been devoted to the complementary problem of determining the necessary structural strength given the loads. However, in our opinion, this is in fact the problem in which the power of limit analysis comes to its full right, and most clearly outperforms incremental elasto-plastic analysis. An example of this is the design of reinforced concrete slabs. Here the material strength if governed by the two orthogonal layers of reinforcement at the top and bottom of the slab, and thus, the design of such a structure requires the determination of four independent strength parameters. This problem has previously been treated numerically by among others Damkilde and Høyer [1], Krenk et al. [2], Damkilde and Krenk [3], and Krabbenhoft and Damkilde [4]. Also reinforced concrete structures loaded in their own plane have been considered, Poulsen and Damkilde [5].

Whereas the upper bound method is usually preferred in hand calculations the lower bound method has some obvious advantages when it comes to numerical computations. One of the most significant of these is the ease with which the method is generalized to include all the common structural elements known from elastic analysis. This generalization comes about by adopting the well-known finite element concept. In contrast to most elastic finite element formulations the elements are stress based rather then displacement based. With the stresses as the variables a set of equilibrium equations can be formulated. Additionally, a set of relevant yield conditions are imposed, and the task then consists of minimizing or maximizing some function subject to these conditions. In load optimization the quantity to be maximized is the magnitude of the load set, whereas in material optimization some function representing the overall cost of the structure is minimized. If all equilibrium, boundary, and yield conditions are satisfied the resulting solution is safe, which is of course another desirable feature.

An important aspect of computational limit analysis is the efficiency of the optimization algorithm. Whereas the simplex method was popular in many of the earlier works, other much more efficient methods have recently been developed, see e.g. Borges et al. [6], Lyamin [7] and Krabbenhoft and Damkilde [8]. The common feature of these algorithms is that linear as well as nonlinear constraints can be included in the optimization problem. Furthermore, the number of iterations required, typically 20–50, is largely independent of the problem size, and since each iteration requires more or less the same as the solution of an equivalent system of elastic finite element equations, problems containing tens of thousands of variables can be solved in a matter of a few minutes.

2.1. Lower bound method—load optimization

Using the lower bound theorem for load optimization the aim is to find a stress distribution which maximizes the intensity of a predefined set of external loads. The stress distribution must be statically admissible, i.e. all equilibrium equations and yield conditions must be fulfilled. For a discrete structure the equilibrium equations can be written in matrix notation as

$$\boldsymbol{E}\boldsymbol{\sigma} = \alpha\boldsymbol{R} + \boldsymbol{R}_{\mathrm{c}} \tag{1}$$

Here $\boldsymbol{E}$ is an equilibrium matrix of n columns and m rows, $\boldsymbol{\sigma}$ is a vector containing the n stress parameters, and the external load consists of a constant part $\boldsymbol{R}_{\mathrm{c}}$ and a part $\boldsymbol{R}$ proportional to a scalar load parameter α. Usually the number of stress variables exceeds the number of equilibrium equations corresponding to the structure being statically indeterminate. As in all finite element procedures the equilibrium matrix and the load vectors are assembled from local element contributions, see Damkilde and Høyer [1].

To prevent violation of the yield criteria an additional set of restrictions must be included. These can be written as

$$f_j(\boldsymbol{\sigma},\boldsymbol{\mu}) \leqslant 0, \quad j = 1,2,\ldots,p \tag{2}$$

where $\boldsymbol{\mu}$ are predefined strength parameters. These restrictions will for all but the simplest structures be of a nonlinear nature, but can usually be linearized in a straight-forward manner.

With these two sets of constraints, linear equilibrium equations and nonlinear yield criteria inequalities, the lower bound load optimization problem can be written as

$$\begin{aligned} &\text{maximize} && \alpha \\ &\text{subject to} && \boldsymbol{E\sigma} = \alpha\boldsymbol{R} + \boldsymbol{R}_c \\ &&& f_j(\boldsymbol{\sigma},\boldsymbol{\mu}) \leqslant 0, \quad j = 1,2,\ldots,p \end{aligned} \tag{3}$$

2.2. Lower bound method—material optimization

In material optimization the external loads are known and the aim is again to find an optimal stress distribution, but now such that the overall cost of the structure is minimized. As a measure of the cost a weighted sum of the strength parameters appearing in the yield criterion is often used. This problem can be written as

$$\begin{aligned} &\text{minimize} && \boldsymbol{w}^T\boldsymbol{\mu} \\ &\text{subject to} && \boldsymbol{E\sigma} = \boldsymbol{R} \\ &&& f_j(\boldsymbol{\sigma},\boldsymbol{\mu}) \leqslant 0, \quad j = 1,2,\ldots,p \end{aligned} \tag{4}$$

where $\boldsymbol{w}$ is a vector of weighting factors. The objective function can of course be supplemented with other relevant quantities such as a weighted sum of certain boundary stresses if the objective is to reduce the cost of supports. Furthermore, the material optimization problem is readily extended to include multiple load cases, see Damkilde and Høyer [1].

2.2.1. Sheet pile wall design

As mentioned earlier the quantities to be determined in the design of sheet pile walls are the necessary yield moment, the anchor force and the wall depth. In principle an optimization problem minimizing a weighted sum of these quantities could be formulated. However, from a numerical point of view, the solution to such a problem, which is most likely non-convex, would be extremely difficult. Furthermore, the choice of weighting factors is not particularly obvious. To simplify matters we propose a two-phase method. In the first phase the yield moment of each wall segment is an independent design variable, and the sum of yield moments is then minimized. This gives a good estimate of the necessary wall depth since yield moments approximately equal to zero will be chosen below the necessary depth. The second phase then consists of determining the necessary yield moment given the wall depth, this time with one common design variable for all wall segments.

In the computations anchors are included by allowing for a shear stress discontinuity in the wall in the anchorage point, and the anchor force is then determined a posteriori on the basis of equilibrium.

3. Finite element discretization

The finite element discretization must be performed to allow for three different types of equilibrium equations to be satisfied. Equilibrium of a soil element is described by

$$\frac{\partial\sigma_x}{\partial x} + \frac{\partial\tau_{xy}}{\partial y} = 0 \tag{5}$$

$$\frac{\partial\sigma_y}{\partial y} + \frac{\partial\tau_{xy}}{\partial x} = \gamma \tag{6}$$

where γ is the downward directed unit weight of the soil, and x and y define a usual Cartesian coordinate system as shown in Fig. 1.

The sheet pile wall must satisfy both transverse and longitudinal equilibrium, i.e.

$$\frac{\mathrm{d}^2M}{\mathrm{d}y^2} = p(y) \tag{7}$$

and

$$\frac{\mathrm{d}N}{\mathrm{d}y} = q(y) \tag{8}$$

where p and q are transverse and longitudinal line loads respectively.

Thus, the types of finite elements needed are plate elements for (5) and (6), beam elements for (7) and truss elements for (8). In the following we adopt the elements used by Poulsen and Damkilde [5] for the analysis of reinforced concrete structures. These elements allow for the equilibrium equations to be satisfied exactly such that true lower bound solutions can be obtained.

3.1. Plate element

The plate element, shown in Fig. 2, enables a linear variation of the stresses. In contrast to most displacement finite element formulations the variables, in this case the stresses, are ascribed to the local nodes of the individual elements rather than to the nodes of the global mesh. The discontinuous stress fields that may appear as a result of this discretization are rendered statically admissible by requiring continuity in the normal and shear forces across element interfaces, see Fig. 2. Since the stress variation is linear these conditions must be imposed in two points along each element interface.

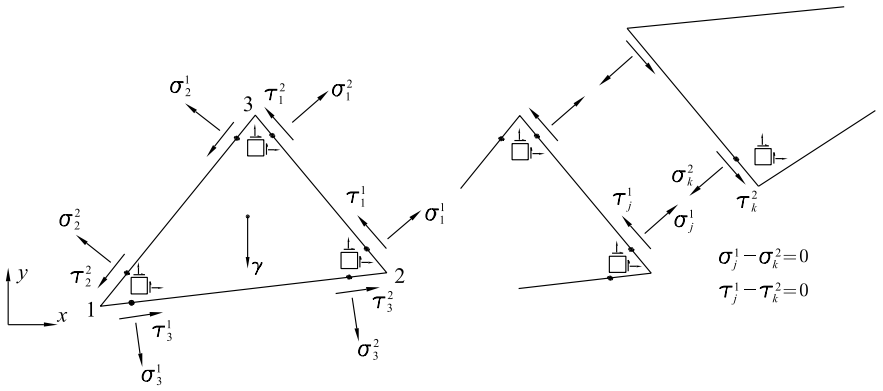

Fig. 2. Lower bound plate element and statically admissible stress discontinuity.

The stress distributions are interpolated by means of area coordinates ξ_j as

$$\sigma_x = \sum_{j=1}^{3} \xi_j \sigma_x^j, \quad \sigma_y = \sum_{j=1}^{3} \xi_j \sigma_y^j, \quad \tau_{xy} = \sum_{j=1}^{3} \xi_j \tau_{xy} \tag{9}$$

Using the differentiation rules for area coordinates the equilibrium equations (5) and (6) can be written as

$$\frac{t}{2A} \sum_{j=1}^{3} \begin{bmatrix} b_j & 0 & -a_j \\ 0 & -a_j & b_j \end{bmatrix} \begin{bmatrix} \sigma_x^j \\ \sigma_y^j \\ \tau_{xy}^j \end{bmatrix} + \begin{bmatrix} 0 \\ \gamma \end{bmatrix} = \begin{bmatrix} 0 \\ 0 \end{bmatrix} \tag{10}$$

where A is the triangle area, t the thickness, and $a_j = x_{j+1} - x_{j-1}$, $b_j = y_{j+1} - y_{j-1}$, where $j = 1,2,3$ refers to the nodes numbers.

With the sign convention shown in Fig. 2 the normal and shear forces are given by

$$\begin{bmatrix} \sigma_k^\beta \\ \tau_k^\beta \end{bmatrix} = \frac{1}{l_k^2} \begin{bmatrix} b_k^2 & a_k^2 & -2a_k b_k \\ a_k b_k & -a_k b_k & b_k^2 - a_k^2 \end{bmatrix} \begin{bmatrix} \sigma_x^{k+\delta} \\ \sigma_y^{k+\delta} \\ \tau_{xy}^{k+\delta} \end{bmatrix},$$

$$\delta = \begin{cases} +1 & \text{for } \beta = 1 \\ -1 & \text{for } \beta = 2 \end{cases} \tag{11}$$

where l_k is the length of side k. The value of β, 1 or 2, refers to the beginning and end of each side respectively. These shear and normal stresses are used to enforce equilibrium across element interfaces as well as to couple the plate element with the beam and truss elements.

3.2. Truss element

The normal stress distribution in the sheet pile wall is modeled by means of truss elements. The truss elements are coupled to the plate elements via the shear stress distributions along the sides of the plate elements as shown in Fig. 3. Since the shear stress distribution along the plate edges is linear a quadratic interpolation of the normal force in the truss element is needed in order to satisfy (8) exactly. Thus, the normal force is interpolated as

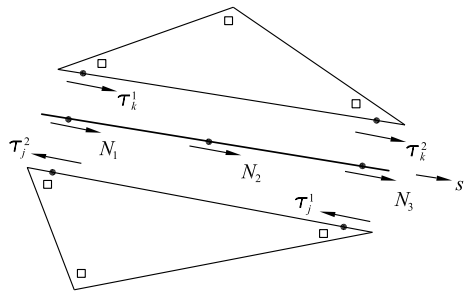

Fig. 3. Coupling between truss and plate elements.

$$N = (1-s)(1-2s)N_1 + 4s(1-s)N_2 + s(2s-1)N_3 \tag{12}$$

where $s \in [0;1]$ is shown in Fig. 3. The equilibrium equation (8) can then be written as

$$\frac{1}{l} \begin{bmatrix} -3 & 4 & -1 \\ 1 & -4 & 3 \end{bmatrix} \begin{bmatrix} N_1 \\ N_2 \\ N_3 \end{bmatrix} = t \begin{bmatrix} \tau_k^1 - \tau_j^2 \\ \tau_k^2 - \tau_j^1 \end{bmatrix} \tag{13}$$

where l is the length of the element. In addition to these equilibrium conditions, force equilibrium in each node is imposed.

3.3. Beam element

Whereas the truss element couples with the plate edge shear stresses, the beam element couples with the normal stresses. Thus, in order to enable exact fulfillment of (7) a cubic moment interpolation is necessary. Using the notation defined previously the equilibrium equation (7) can be written in discrete form as

$$\frac{1}{l^2}\begin{bmatrix} 18 & -45 & 36 & -9 \\ -9 & 36 & -45 & 18 \end{bmatrix}\begin{bmatrix} M_1 \\ M_2 \\ M_3 \\ M_4 \end{bmatrix} = t\begin{bmatrix} \sigma_k^1 - \sigma_j^2 \\ \sigma_k^2 - \sigma_j^1 \end{bmatrix} \tag{14}$$

Again, conditions ensuring nodal equilibrium must be imposed. This is done by requiring moment and force equilibrium in each node, where the two nodal force equilibrium equations consist of contributions from both the truss normal force and the beam shear force. The shear forces at each end of the element are given by

$$\begin{bmatrix} V_0 \\ V_l \end{bmatrix} = \frac{1}{2l}\begin{bmatrix} -11 & 18 & -9 & 2 \\ -2 & 9 & -18 & 11 \end{bmatrix}\begin{bmatrix} M_1 \\ M_2 \\ M_3 \\ M_4 \end{bmatrix} \tag{15}$$

3.4. Total equilibrium

The total equilibrium system for a general plate–beam–truss system comprises the global and local equilibrium equations as well as coupling conditions connecting the different types of elements. The total system can be written as

$$\begin{matrix} \text{Global equilibrium} \\ \text{Local equilibrium} \\ \text{Plate-beam-truss coupling} \end{matrix}\left\{\begin{array}{ccc} \boldsymbol{E}_{\mathrm{p}}^{\mathrm{g}} & \boldsymbol{0} & \boldsymbol{0} \\ \boldsymbol{0} & \boldsymbol{E}_{\mathrm{b}}^{\mathrm{g}} & \boldsymbol{0} \\ \boldsymbol{0} & \boldsymbol{0} & \boldsymbol{E}_{\mathrm{p}}^{\mathrm{g}} \\ \hline \boldsymbol{E}_{\mathrm{p}}^{\mathrm{l}} & \boldsymbol{0} & \boldsymbol{0} \\ \boldsymbol{0} & \boldsymbol{E}_{\mathrm{b}}^{\mathrm{l}} & \boldsymbol{0} \\ \boldsymbol{0} & \boldsymbol{E}_{\mathrm{bt}}^{\mathrm{l}} & \boldsymbol{E}_{\mathrm{tb}}^{\mathrm{l}} \\ \hline \boldsymbol{E}_{\mathrm{pb}} & \boldsymbol{E}_{\mathrm{bp}} & \boldsymbol{0} \\ \boldsymbol{E}_{\mathrm{pt}} & \boldsymbol{0} & \boldsymbol{E}_{\mathrm{tp}} \end{array}\right]\begin{bmatrix} \boldsymbol{\sigma} \\ \boldsymbol{M} \\ \boldsymbol{N} \end{bmatrix} = \left[\begin{array}{c} \hat{\boldsymbol{\gamma}} \\ \hat{\boldsymbol{p}} \\ \hat{\boldsymbol{q}} \\ \hline \hat{\boldsymbol{\sigma}} \\ \widehat{\boldsymbol{M}} \\ \widehat{\boldsymbol{P}} \\ \hline \boldsymbol{0} \\ \boldsymbol{0} \end{array}\right] \tag{16}$$

Here $\hat{\boldsymbol{\gamma}}$, $\hat{\boldsymbol{p}}$, $\hat{\boldsymbol{q}}$ are prescribed plate body loads, transverse beam loads and longitudinal truss loads respectively, and $\hat{\boldsymbol{\sigma}}$, $\widehat{\boldsymbol{M}}$ and $\widehat{\boldsymbol{P}}$ are prescribed plate edge stresses, nodal beam moments and beam–truss nodal forces respectively. The global equilibrium equations correspond to (5)–(8) whereas the local equilibrium conditions ensure continuity between plate elements and moment and force equilibrium in each node of the beam–truss system. Furthermore, the plate edge shear and normal forces couple with the beam and truss elements respectively. In a more compact form the full equilibrium system can be written as

$$\boldsymbol{E}_{\mathrm{p}}\boldsymbol{\sigma} + \boldsymbol{E}_{\mathrm{b}}\boldsymbol{M} + \boldsymbol{E}_{\mathrm{t}}\boldsymbol{N} = \boldsymbol{R} \tag{17}$$

In addition to these equilibrium conditions it may also be necessary to include equilibrium inequalities. For the sheet pile wall, for example, a downward directed resulting normal force is required. Also, inequalities are needed in specifying the roughness of the wall, i.e. the magnitude of the shear that can be transferred between plate and truss elements. Similarly to (17) a general set of equations describing these conditions can be written as

$$\boldsymbol{A}_{\mathrm{p}}\boldsymbol{\sigma} + \boldsymbol{A}_{\mathrm{b}}\boldsymbol{M} + \boldsymbol{A}_{\mathrm{t}}\boldsymbol{N} \leqslant \boldsymbol{b} \tag{18}$$

4. Yield conditions

As is common practice in geotechnical analysis of cohesive-frictional soils we assume yielding to be governed by the Mohr–Coulomb yield criterion. Using this criterion in plane strain the stresses must satisfy

$$(\sigma_x - \sigma_y)^2 + 4\tau_{xy}^2 - (2c\cos\phi - (\sigma_x + \sigma_y)\sin\phi)^2 \leqslant 0 \tag{19}$$

where c is the cohesion and ϕ is the angle of friction.

The general yield criterion for a beam subjected to a combination of normal force and moment can be written as

$$f(M, f_{\mathrm{y}}) + g(N, f_{\mathrm{y}}) + k \leqslant 0 \tag{20}$$

where f_{y} is the yield strength. Generally, f, g and k depend on the geometry of the cross section. For rectangular cross sections a commonly used criterion is

$$\left|\frac{N}{N_0}\right| + \left(\frac{M}{M_0}\right)^2 \leqslant 1 \tag{21}$$

where M_0 and N_0 are the plastic moments and normal forces respectively. However, in sheet pile wall design the strength of the wall is usually assumed to be given solely by the bending strength, i.e. the moments are limited by

$$-M_0 \leqslant M \leqslant M_0 \tag{22}$$

In the following this criterion is used.

It should be emphasized that the optimization method used to solve the lower bound material optimization problem is by no means restricted to the above yield criteria. Alternative criteria, e.g. the Drucker–Prager criterion for the soil, are easily implemented.

5. Formulation of design optimization problem

As already discussed the design strategy consists of first minimizing the sum of the wall yield moments with each wall segment being assigned an independent design parameter. This problem can be written as

$$\begin{aligned} &\text{minimize} && \boldsymbol{e}^{\mathrm{T}}\boldsymbol{M}_0 \\ &\text{subject to} && \boldsymbol{E}_{\mathrm{p}}\boldsymbol{\sigma} + \boldsymbol{E}_{\mathrm{b}}\boldsymbol{M} + \boldsymbol{E}_{\mathrm{t}}\boldsymbol{N} = \boldsymbol{R} \\ &&& \boldsymbol{A}_{\mathrm{p}}\boldsymbol{\sigma} + \boldsymbol{A}_{\mathrm{b}}\boldsymbol{M} + \boldsymbol{A}_{\mathrm{t}}\boldsymbol{N} \leqslant \boldsymbol{b} \\ &&& \boldsymbol{f}(\boldsymbol{\sigma}) \leqslant \boldsymbol{0} \\ &&& \boldsymbol{M} \leqslant \boldsymbol{M}_0 \\ &&& \boldsymbol{M} \geqslant -\boldsymbol{M}_0 \end{aligned} \tag{23}$$

Here the functions $\boldsymbol{f}(\boldsymbol{\sigma})$ define the Mohr–Coulomb criterion imposed in each plate stress point, $\boldsymbol{e}$ is a vector of ones and $\boldsymbol{M}_0$ is a vector containing the design yield moments. The solution to this optimization problem gives a good indication of the necessary wall depth as yield moments approximately equal to zero will be found below the necessary depth.

Next, with the wall depth known, the phase two problem then consists of finding the necessary yield moment with all wall segments being assigned a common design parameter. This problem is written as

$$\begin{aligned} &\text{minimize} && M_0 \\ &\text{subject to} && \boldsymbol{E}_{\mathrm{p}}\boldsymbol{\sigma} + \boldsymbol{E}_{\mathrm{b}}\boldsymbol{M} + \boldsymbol{E}_{\mathrm{t}}\boldsymbol{N} = \boldsymbol{R} \\ &&& \boldsymbol{A}_{\mathrm{p}}\boldsymbol{\sigma} + \boldsymbol{A}_{\mathrm{b}}\boldsymbol{M} + \boldsymbol{A}_{\mathrm{t}}\boldsymbol{N} \leqslant \boldsymbol{b} \\ &&& \boldsymbol{f}(\boldsymbol{\sigma}) \leqslant \boldsymbol{0} \\ &&& \boldsymbol{M} \leqslant \boldsymbol{e}M_0 \\ &&& \boldsymbol{M} \geqslant -\boldsymbol{e}M_0 \end{aligned} \tag{24}$$

6. Solution of optimization problem

The solution of the optimization problem is realized by employing an interior point algorithm which has proven to be very efficient with respect to the load optimization problem, Krabbenhoft and Damkilde [8]. Since the material optimization problem is very similar in structure—linear objective, nonlinear equalities and linear equalities—a similar efficiency should be expected in the case of material optimization. In the following the solution algorithm is outlined with reference to the general material optimization problem (4).

$$\begin{aligned} &\text{minimize} && \boldsymbol{w}^{\mathrm{T}}\boldsymbol{\mu} \\ &\text{subject to} && \boldsymbol{E}\boldsymbol{\sigma} = \boldsymbol{R} \\ &&& \boldsymbol{f}(\boldsymbol{\sigma},\boldsymbol{\mu}) \leqslant \boldsymbol{0} \end{aligned} \tag{25}$$

The inequalities are first converted into equalities by addition of positively restricted slack variables $\boldsymbol{s}$. Next, these slack variables are included into the objective via a logarithmic barrier function such that no explicit reference to the positivity of the slack variables is needed. The modified problem is then

$$\begin{aligned} &\text{minimize} && \boldsymbol{w}^{\mathrm{T}}\boldsymbol{\mu} - \rho^k \sum_{j=1}^{p} \log s_j \\ &\text{subject to} && \boldsymbol{E}\boldsymbol{\sigma} = \boldsymbol{R} \\ &&& \boldsymbol{f}(\boldsymbol{\sigma},\boldsymbol{\mu}) + \boldsymbol{s} = \boldsymbol{0} \end{aligned} \tag{26}$$

where ρ^k is a parameter which should be reduced as the solution is approached.

The Lagrangian of (26) is given by

$$\begin{aligned} \mathscr{L} = {} & \boldsymbol{w}^{\mathrm{T}}\boldsymbol{\mu} - \rho^k \sum_{j=1}^{p} \log s_j + \boldsymbol{v}^{\mathrm{T}}(\boldsymbol{R} - \boldsymbol{E}\boldsymbol{\sigma}) \\ & + \boldsymbol{\lambda}^{\mathrm{T}}(\boldsymbol{f}(\boldsymbol{\sigma},\boldsymbol{\mu}) + \boldsymbol{s}) \end{aligned} \tag{27}$$

where $\boldsymbol{v}$ and $\boldsymbol{\lambda}$ are Lagrange multipliers. Since (26) is a convex program by virtue of the yield conditions being convex and all other restrictions linear, the solution to the optimization problem can be found by solving the first order Kuhn–Tucker conditions, see e.g. Nash and Sofer [9], which state that the first order derivatives of the Lagrangian should vanish at the optimum. This leads to the following conditions

$$\boldsymbol{E}^{\mathrm{T}}\boldsymbol{v} - \nabla_{\sigma}\boldsymbol{f}\ \boldsymbol{\lambda} = \boldsymbol{0} \tag{28}$$

$$\boldsymbol{w} + \nabla_{\mu}\boldsymbol{f}\ \boldsymbol{\lambda} = \boldsymbol{0} \tag{29}$$

$$\boldsymbol{S}\boldsymbol{\lambda} = \rho^k \boldsymbol{e} \tag{30}$$

$$\boldsymbol{f}(\boldsymbol{\sigma},\boldsymbol{\mu}) + \boldsymbol{s} = \boldsymbol{0} \tag{31}$$

$$\boldsymbol{E}\boldsymbol{\sigma} - \boldsymbol{R} = \boldsymbol{0} \tag{32}$$

together with the positivity requirements on $\boldsymbol{s}$ and $\boldsymbol{\lambda}$.

6.1. Duality between upper and lower bound methods

The duality between the upper and lower bound theorems of plasticity has an analogy in the duality theory of mathematical programming. With a problem origi-

nally formulated as a minimization problem one can construct a dual maximization problem with the same objective value as the original problem, but with the variables being different in each problem. In the framework of discrete limit analysis this means that from a problem originally formulated as lower bound it is possible to construct the corresponding approximate upper bound problem. In load optimization this duality property has a clear physical interpretation since the upper and lower bound problems can be formulated independently of each other and then by means of duality shown to be equivalent.

However, when it comes to material optimization the natural starting point for formulating the problem is the lower bound theorem whereas an upper bound material optimization problem can only be formulated indirectly. Considering the lower bound problem (25) a linearization can be obtained by replacing the nonlinear inequalities by their first order Taylor expansion around points $(\boldsymbol{\sigma}^*, \boldsymbol{\mu}^*)$ lying on the yield surface, i.e.

$$\begin{aligned} \boldsymbol{f}(\boldsymbol{\sigma},\boldsymbol{\mu}) &\simeq \boldsymbol{f}(\boldsymbol{\sigma}^*,\boldsymbol{\mu}^*) + \nabla_\sigma \boldsymbol{f}^{\mathrm{T}}(\boldsymbol{\sigma}-\boldsymbol{\sigma}^*) + \nabla_\mu \boldsymbol{f}^{\mathrm{T}}(\boldsymbol{\mu}-\boldsymbol{\mu}^*) \\ &= \nabla_\sigma \boldsymbol{f}^{\mathrm{T}}(\boldsymbol{\sigma}-\boldsymbol{\sigma}^*) + \nabla_\mu \boldsymbol{f}^{\mathrm{T}}(\boldsymbol{\mu}-\boldsymbol{\mu}^*) \end{aligned} \tag{33}$$

where the last equality comes about by the fact that $\boldsymbol{f}(\boldsymbol{\sigma}^*, \boldsymbol{\mu}^*) = \boldsymbol{0}$. The linearized material optimization problem is then

$$\begin{aligned} &\text{minimize} && \boldsymbol{w}^{\mathrm{T}}\boldsymbol{\mu} \\ &\text{subject to} && \boldsymbol{E}\boldsymbol{\sigma} = \boldsymbol{R} \\ & && \nabla_\sigma \boldsymbol{f}^{\mathrm{T}}(\boldsymbol{\sigma}-\boldsymbol{\sigma}^*) + \nabla_\mu \boldsymbol{f}^{\mathrm{T}}(\boldsymbol{\mu}-\boldsymbol{\mu}^*) \leqslant \boldsymbol{0} \end{aligned} \tag{34}$$

The dual to this problem is, see e.g. [9],

$$\begin{aligned} &\text{maximize} && \boldsymbol{R}^{\mathrm{T}}\boldsymbol{v} - (\nabla_\sigma \boldsymbol{f}^{\mathrm{T}}\boldsymbol{\sigma}^* + \nabla_\mu \boldsymbol{f}^{\mathrm{T}}\boldsymbol{\mu}^*)^{\mathrm{T}}\boldsymbol{\lambda} \\ &\text{subject to} && \boldsymbol{E}^{\mathrm{T}}\boldsymbol{v} - \nabla_\sigma \boldsymbol{f}^{\mathrm{T}}\boldsymbol{\lambda} = \boldsymbol{0} \\ & && \boldsymbol{w} + \nabla_\mu \boldsymbol{f}^{\mathrm{T}}\boldsymbol{\lambda} = \boldsymbol{0} \end{aligned} \tag{35}$$

This is the upper bound material optimization problem. The displacements at collapse (velocities) are contained in the vector $\boldsymbol{v}$ and $\boldsymbol{\lambda}$ contains the plastic multipliers. The quantity to be minimized is the external work minus some constant contribution from the internal work while the magnitude of the total internal work is limited. As in the upper bound load optimization problem compatibility between displacements and strains is required. These constraints correspond to the optimality conditions (29) and (28) respectively. The optimality conditions (31) and (32) correspond to the yield and equilibrium restrictions stated in the original lower bound material optimization problem (25). The conditions linking the variables of the two problems are expressed by the complementary slackness conditions (30) which, by the use of (28) and (29) and (31) and (32), are easily shown to be equivalent to requiring that the difference between the objectives in (25) and (35) vanishes.

It is a rather peculiar fact that the material strengths do not enter directly into the upper bound material optimization problem, but rather must be determined as the dual variables to this problem. This seems to exclude the upper bound material optimization problem from practical use, since e.g. additional requirements on the design variables cannot be imposed directly but only through duality. The duality between the two problem is, however, useful in determining the displacements at collapse. This will be utilized in the following. For further details on upper/lower bound duality we refer to Krenk et al. [2] and Krabbenhoft and Damkilde [8].

6.2. Solution algorithm

The Kuhn–Tucker conditions (28)–(32) are solved by applying Newton's method. In this way increments of the variables are computed by solution of

$$\begin{bmatrix} \boldsymbol{W}_\sigma & \boldsymbol{0} & \nabla_\sigma \boldsymbol{f} & \boldsymbol{0} & \boldsymbol{E}^{\mathrm{T}} \\ \boldsymbol{0} & \boldsymbol{W}_\mu & \nabla_\mu \boldsymbol{f} & \boldsymbol{0} & \boldsymbol{0} \\ \boldsymbol{0} & \boldsymbol{0} & \boldsymbol{\Lambda} & \boldsymbol{S} & \boldsymbol{0} \\ \nabla_\sigma \boldsymbol{f}^{\mathrm{T}} & \nabla_\mu \boldsymbol{f}^{\mathrm{T}} & \boldsymbol{I} & \boldsymbol{0} & \boldsymbol{0} \\ \boldsymbol{E} & \boldsymbol{0} & \boldsymbol{0} & \boldsymbol{0} & \boldsymbol{0} \end{bmatrix} \begin{bmatrix} \Delta\boldsymbol{\sigma} \\ \Delta\boldsymbol{\mu} \\ \Delta\boldsymbol{s} \\ \Delta\boldsymbol{\lambda} \\ \Delta\boldsymbol{v} \end{bmatrix} = - \begin{bmatrix} \boldsymbol{E}^{\mathrm{T}}\boldsymbol{v} + \nabla_\sigma \boldsymbol{f}\,\boldsymbol{\lambda} \\ \boldsymbol{w} + \nabla_\mu \boldsymbol{f}\,\boldsymbol{\lambda} \\ \boldsymbol{S}\boldsymbol{\lambda} - \rho^k \boldsymbol{e} \\ \boldsymbol{f}(\boldsymbol{\sigma},\boldsymbol{\mu}) + \boldsymbol{s} \\ \boldsymbol{E}\boldsymbol{\sigma} - \boldsymbol{R} \end{bmatrix} \tag{36}$$

where

$$\boldsymbol{W}_\sigma = \sum_{j=1}^{p} \lambda_j \nabla^2_{\sigma\sigma} \boldsymbol{f}(\boldsymbol{\sigma},\boldsymbol{\mu}), \quad \boldsymbol{W}_\mu = \sum_{j=1}^{p} \lambda_j \nabla^2_{\mu\mu} \boldsymbol{f}(\boldsymbol{\sigma},\boldsymbol{\mu}) \tag{37}$$

$$\boldsymbol{S} = \operatorname{diag}(\boldsymbol{s}), \quad \boldsymbol{\Lambda} = \operatorname{diag}(\boldsymbol{\lambda}), \quad \boldsymbol{I} = \operatorname{diag}(\boldsymbol{1}) \tag{38}$$

The algorithm starts at an initial solution $(\boldsymbol{\sigma}^0, \boldsymbol{\mu}^0, \boldsymbol{s}^0, \boldsymbol{\lambda}^0, \boldsymbol{v}^0)$ from which an initial barrier parameter is computed as

$$\rho^0 = \theta(\boldsymbol{s}^0)^{\mathrm{T}}\boldsymbol{\lambda}^0/p, \quad 0 \leqslant \theta \leqslant 1 \tag{39}$$

where p is the number of inequality constraints. The algorithm then proceeds by computing an increment and finally the variables are updated such that $\boldsymbol{s}$ and $\boldsymbol{\lambda}$ remain positive throughout the iterations. At the beginning of each iteration the barrier parameter ρ^k is reduced according to (39) or similar rules.

Further details on the practical implementation of the algorithm can be found in Krabbenhoft and Damkilde [8].

6.2.1. Detecting infeasibility

If the wall depth, estimated on the basis of the phase one problem (23), is not sufficient a situation where there

is no solution to the phase two problem (24) will occur. This may cause severe numerical problems in the optimization algorithm since convergence will never be obtained and the algorithm thus never terminated. To avoid this situation we impose a slightly different set of equilibrium equations and at the same time alter the objective function such that the resulting problem can be written as

$$\begin{aligned} \text{minimize} \quad & M_0 + L(\boldsymbol{y}^+ - \boldsymbol{y}^-) \\ \text{subject to} \quad & \boldsymbol{E}_\mathrm{p}\boldsymbol{\sigma} + \boldsymbol{E}_\mathrm{b}\boldsymbol{M} + \boldsymbol{E}_\mathrm{t}\boldsymbol{N} + \boldsymbol{y}^+ + \boldsymbol{y}^- = \boldsymbol{R} \\ & \boldsymbol{A}_\mathrm{p}\boldsymbol{\sigma} + \boldsymbol{A}_\mathrm{b}\boldsymbol{M} + \boldsymbol{A}_\mathrm{t}\boldsymbol{N} + \boldsymbol{y}^+ + \boldsymbol{y}^- \leqslant \boldsymbol{b} \\ & \boldsymbol{f}(\boldsymbol{\sigma}) \leqslant \boldsymbol{0} \\ & \boldsymbol{M} \leqslant \boldsymbol{e}M_0 \\ & \boldsymbol{M} \geqslant -\boldsymbol{e}M_0 \\ & \boldsymbol{y}^+ \geqslant \boldsymbol{0}, \quad \boldsymbol{y}^- \leqslant \boldsymbol{0} \end{aligned} \tag{40}$$

As seen the equilibrium equations need not be satisfied and thus, a solution should always exist. To force the equilibrium equations to be satisfied if at all possible, equilibrium violations are punished in the objective function by some large number L. Other methods of detecting infeasibility may also be used, see e.g. Nash and Sofer [9].

7. Examples

In the following we consider the sheet pile wall shown in Fig. 1 with $\gamma = 18$ kN/m above level 6.00 m and $\gamma = 10$ kN/m below. In the entire domain the strength parameters of the soil are $c' = 0$ and $\phi' = 30°$ corresponding to sand. Both rough and smooth cantilever and anchored walls are considered. First the problem of determining the necessary yield moment given the wall depth is solved and secondly the procedure for determining the wall depth as well as the necessary yield moment is illustrated.

7.1. Determination of necessary yield moment

Four different walls are considered. All walls have first been designed by Brinch Hansen's method [10] giving the necessary yield moment, wall depth and anchor force, if any. The wall depth thus determined is then used in the lower bound computations where the aim is to determine the necessary yield moment. In Brinch Hansen's method a rupture figure corresponding to an probable failure mode of the wall is postulated. This rupture figure can consist of straight lines and circles and the stress distribution can then be determined by integration of Kötter's equation. To simplify the computations Brinch Hansen introduced the equivalent earth pressure coefficients. As an approximation linear pressure distributions were assumed which, strictly speaking, is only valid in the case of zone rupture. Moreover, some of the rupture figures used are not statically admissible and circular rupture lines are only kinematically admissible in the case of $\phi = 0$. Thus, the solutions obtained by the method are neither true upper or lower bounds.

7.1.1. Cantilever walls

The results for the cantilever walls are shown in Table 1. As seen the agreement with Brinch Hansen's method is rather good. For the rough wall the lower bound method predicts a necessary yield moment which is approximately 3% larger than what Brinch Hansen's method suggests, while for the smooth wall the auto-

Table 1
Necessary yield moments (kN m/m) for cantilever walls

	Rough, $d_\mathrm{w} = -6.26$ m		Smooth, $d_\mathrm{w} = -9.60$ m	
	Lower bound	Brinch Hansen	Lower bound	Brinch Hansen
Mom.	576	560	982	985

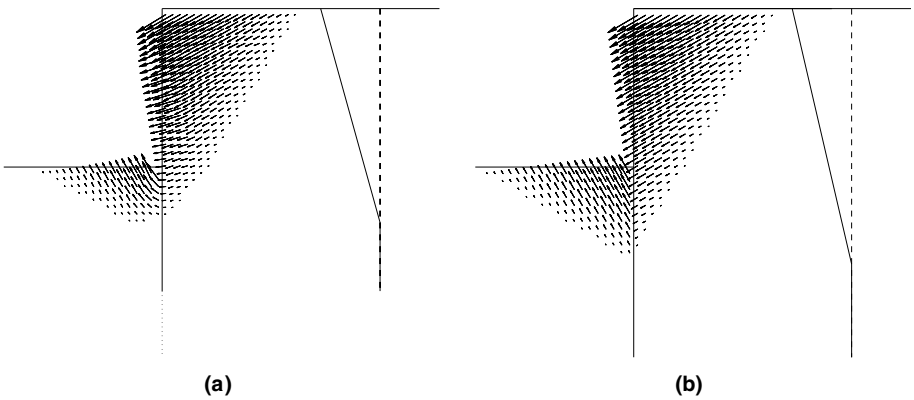

Fig. 4. Velocity fields for rough (a) and smooth (b) cantilever walls. The wall rupture mechanisms are shown to the right in each figure.

mated lower bound method predicts a slightly lower yield moment than the hand calculation method.

The velocity fields derived by means of duality are shown in Fig. 4(a) and (b). As expected the velocities define a P-rupture for the rough wall and an R-rupture for the smooth wall. On the active side the angle between the rupture lines and the ground should be $45° + \phi/2 = 60°$ and on the passive side $45° - \phi/2 = 30°$. This is fulfilled to within the accuracy with which we can measure.

7.1.2. Anchored walls

An anchor is now placed at level 7.00 m. This dramatically reduces the necessary yield moment as well as the wall depth. The results are shown in Table 2.

Table 2
Necessary yield moments (kN m/m) and anchor forces (kN/m)

	Rough, $d_w = -2.00$ m		Smooth, $d_w = -3.27$ m	
	Lower bound	Brinch Hansen	Lower bound	Brinch Hansen
Mom.	115	125	174	182
Anch.	112	75	146	105

Again the necessary lower bound yield moments follow those of Brinch Hansen with the latter being approximately 5–8% larger than those predicted by the former method. The anchor forces, however, deviate significantly with the lower bound method suggesting forces up to 40% larger than those of Brinch Hansen. The velocity fields are shown in Fig. 5(a) and (b). With respect to the corresponding rupture figures it is interesting to note that for walls with yield hinges Brinch Hansen assumed that each wall segment defines an independent rupture figure. For both the rough and the smooth wall traces of two different rupture figures can be seen. For the rough wall the segment below the yield hinge defines a P-rupture while for the smooth wall an R-rupture occurs. For the wall segment above the yield hinge the corresponding rupture figure is harder to categorize. However, the triangular area at the top right of both figures suggests a figure similar to that of AaR-rupture.

7.2. Determination of wall depth and yield moment

In this section the complete design problem is considered. As an example the smooth cantilever wall from

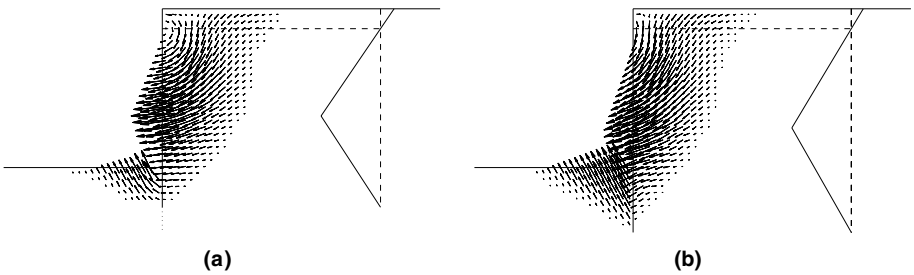

Fig. 5. Velocity fields for rough (a) and smooth (b) anchored walls. The wall rupture mechanisms are shown to the right in each figure.

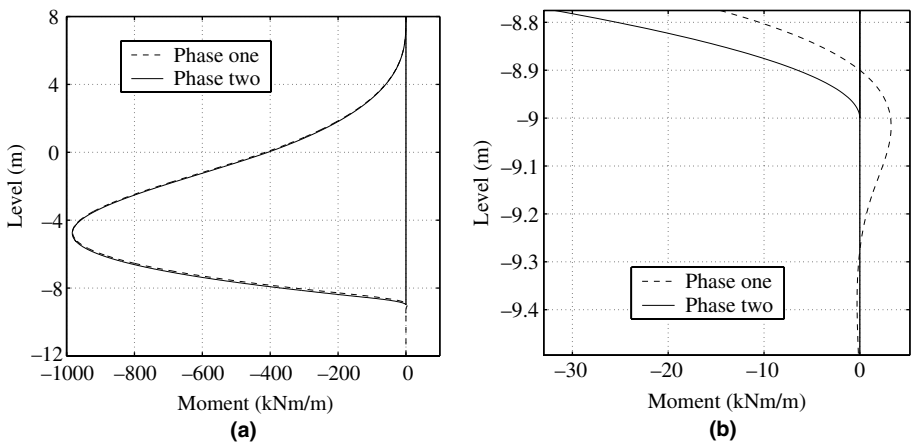

Fig. 6. Moment distributions.

the previous example is taken. In the phase one problem where each yield moment is optimized independently we estimate a necessary depth of 12 m. This results in the moment distribution shown in Fig. 6(a). A zoom of the conditions near the point where the moment becomes zero is shown in Fig. 6(b). As can be seen the moment first becomes zero at around −8.9 m. A good, estimate of the necessary wall depth is therefore 9.00 m. This value is then used in the phase two problem where it is confirmed that the depth is indeed sufficient. The necessary yield moment is found to be 983 kN m/m compared to 982 kN m/m in the first analysis, whereas the wall depth has been reduced by 0.6 m.

In the phase one problem each yield moment is weighted identically. A more realistic weighting, however, would be to increase the weighting factors with the depth such that the cost of ramming would be included directly into the objective. Also the position of the anchor may be taken as a variable, again with the cost increasing as the depth increases.

7.3. Sheet pile wall in layered soil

A more practical example as sketched in Fig. 7 is now considered. The wall is assumed rough and the strength parameters of the soil under drained conditions are given in Table 3. Below the water level the reduced soil weight $\gamma' = \gamma_m - \gamma_w$ is used.

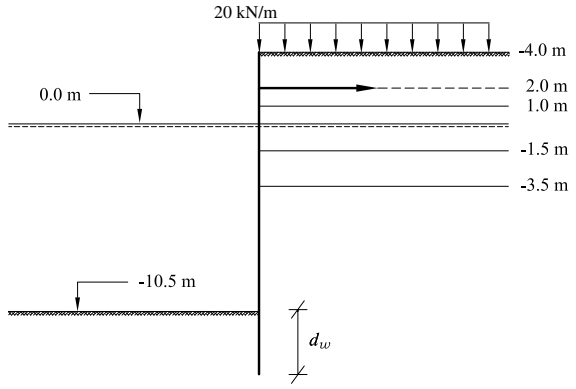

Fig. 7. Sheet pile wall in layered soil.

Table 3
Soil properties

Soil	Level (m)	c'	ϕ'	γ'
Sand I	4.0 – 1.0	0.0	35.0	18.0
Sand I	1.0 – 0.0	0.0	35.0	10.0
Clay I	0.0 – (−1.5)	0.0	30.0	9.0
Clay II	(−1.5) – (−3.5)	15.0	30.0	9.0
Sand II	(−3.5) – (−∞)	0.0	38.0	10.0

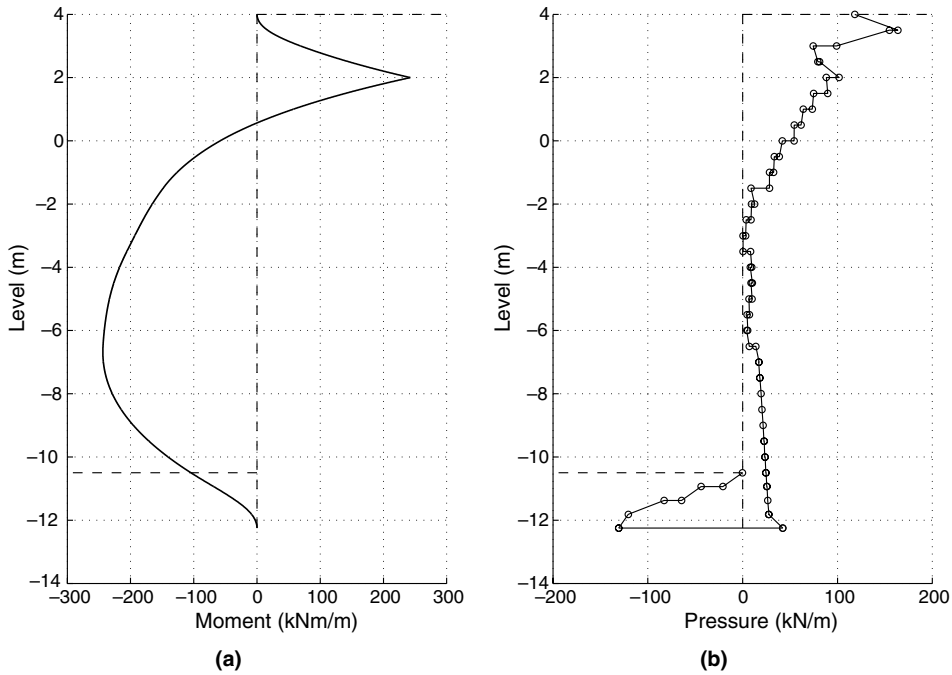

Fig. 8. Moment (a) and earth pressure (b) distributions.

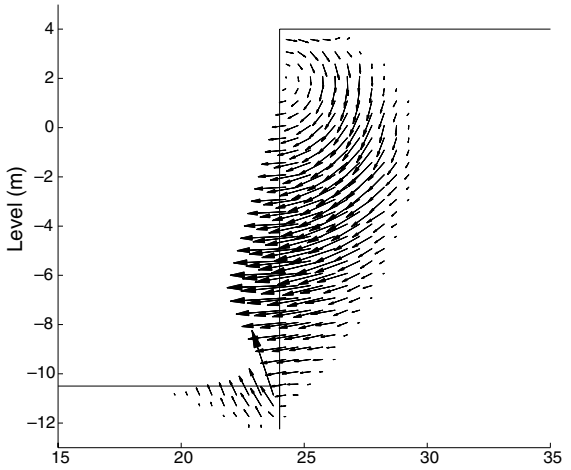

Fig. 9. Velocity field, sheet pile wall in layered soil.

The design of the wall proceeds by estimating a necessary minimum wall depth by a phase–one procedure as described in the previous section. Next, this estimate is confirmed by a minimization of the necessary yield moment of the wall. By this procedure the necessary minimum depth has been found to be close to $d_w = 1.75$ m. The corresponding yield moment and anchor forces were found to be $M = 244$ kN m/m and $A = 446$ kN/m respectively. The moment and earth pressure distributions are shown in Fig. 8. As expected the moment attains its negative maximum at the anchorage point whereas the positive maximum appears around level −7.0 m. The correspondence between the location of this point and velocity field shown in Fig. 9 is good. Here, a rotation about the anchorage point and the presence of a yield hinge at around level −7.0 m are clearly visible. As for the earth pressure distribution a rather non–smooth variation can be observed. This has also been observed for other configurations and also for finer meshes than the one used in the present computation. This may indicate that the results are rather insensitive to the precise variation of earth pressure, i.e. that the computed minimum is quite flat. This is also supported by the iteration counts which are generally somewhat higher than for most other problems with less flat optima. Thus, whereas typical load bearing capacity problems usually require 20–40 iterations, the problems considered here often require 80–100 iterations.

8. Conclusions

The design of sheet pile walls has been considered from a limit analysis material optimization point of view. Both smooth and rough cantilever and anchored walls have been treated. The obtained results have been compared to the classic method of Brinch Hansen and good agreement is generally found. In contrast to this method, however, the present method results in lower bound solutions, i.e. designs which are safe.

In the paper a design procedure where the primary objective is the minimization of the wall yield moment has been developed. However, it is of course entirely possible to construct interaction charts, e.g. with the wall depth and yield moment as variables. This ensures a high degree of flexibility in the design procedure as the combination of the wall depth and the yield moment, which under a particular set of practical constraints are optimal, can be easily chosen on the basis of such charts.

References

[1] Damkilde L, Høyer O. An efficient implementation of limit state calculations based on lower-bound solutions. Comput Struct 1993;49(6):953–62.
[2] Krenk S, Damkilde L, Høyer O. Limit analysis and optimal design of plates with equilibrium elements. J Eng Mech 1994;120(6):1237–54.
[3] Damkilde L, Krenk S. Limits—a system for limit state analysis and optimal material layout. Comput Struct 1997;64(1–4):709–18.
[4] Krabbenhoft K, Damkilde L. Lower bound limit analysis of slabs with nonlinear yield criteria. Comput Struct 2002;80:2043–57.
[5] Poulsen PN, Damkilde L. Limit analysis of reinforced concrete plates subjected to in-plane forces. Int J Solids Struct 2000;37:6011–29.
[6] Borges LA, Zouain N, Huespe AE. A nonlinear optimization procedure for limit analysis. Eur J Mech, A/Solids 1996;15(3):487–512.
[7] Lyamin AV, Sloan SW. Lower bound limit analysis using non-linear programming. Int J Numer Meth Eng 2002; 55:573–611.
[8] Krabbenhoft K, Damkilde L. A general nolinear optimization algorithm for lower bound limit analysis. Int J Numer Meth Eng 2003;56:165–84.
[9] Nash SG, Sofer A. Linear and nonlinear programming. New York, NY: McGraw-Hill; 1996.
[10] Brinch Hansen J. Earth pressure calculation. Copenhagen, Denmark: The Danish Technical Press; 1953.